UNIVERSITY OF CALIFORNIA
SANTA CRUZ

A BIO-MIMETIC LEAF WETNESS SENSOR

A thesis submitted in partial satisfaction of the
requirements for the degree of

MASTER OF SCIENCE

in

ELECTRICAL AND COMPUTER ENGINEERING

by

Brian Nguyen

March 2022

The thesis of Brian Nguyen
is approved:

Professor Marco Rolandi, Chair

Professor Colleen Josephson

Professor Mircea Teodorescu

Peter Biehl
Vice Provost and Dean of Graduate Studies

Table of Contents

List of Figures

List of Tables

Abstract

A Bio-mimetic Leaf Wetness Sensor

by

Brian Nguyen

Leaf wetness duration (LWD) is an important measurement in agricultural meteorology since it is a determining factor to pathogen infection and critical to the rate of plant disease development. Currently, there are commercially available electronic LWD sensors implemented in crop management systems, and, although, these sensors are robust and highly precise, they are unable to fully mimic the surface and wetting properties of real leaves. To mitigate the limitations of commercially available leaf wetness sensors (LWS), I developed a bio-mimetic sensor that closely replicates the surface properties and hydrophilicity of the leaves using a polydimethylsiloxane (PDMS) double-casting technique. Measurements taken from the modified LWS suggest that from three different leaf species, the commercialized LWS is capable of closely matching the wettability of only one of the corresponding leaves. This proof of concept shows that bio-mimetic leaf wetness sensors can better represent plant leaves and, therefore, not only verifies the commercialized LWS's limited effectiveness but also demonstrates the importance of incorporating wettability into future LWS sensor development.

Acknowledgments

I want to thank my supervisor, Marco Rolandi, and other faculty who have made my journey and this project possible. I am appreciative for all of my peers and mentors whom I have learned so much from.

I would like to thank my friends and family who have supported through this journey.

Without everyone none of this would be possible. I am truly grateful.

Chapter 1

Introduction

In 2019, the Food and Agriculture Organization of the United Nations estimated that between 20 to 40 percent of global crop production are lost to plant diseases and pests annually, with plant diseases costing the global economy roughly $220 billion each year [1]. Controls measures to mitigate the impact of plant disease on global agricultural production is therefore necessary. Growers and researchers have developed a wide array of measures for the management of specific plant diseases, and, as a result, disease-warning systems have become a popular method used by growers to preemptively mitigate destructive events using chemical treatment or biological management [2, 3].

Environmental monitoring, particularly humidity and leaf wetness, is especially important. The relationship between leaf wetness duration and plant diseases is a field that first dates to 1853. Debary was one of the first researchers to study the association between the infection of potatoes by *Phytophthora infestans* with occurrence of free water on the plant canopy [4]. Since then, disease-warning systems have progressed to

include other meteorological factors including rainfall, humidity, and air temperature. However, the measurement of leaf wetness duration (LWD) remains a priority due to its governing role in infection processes for many fungal pathogens [5–11].

Fungus	Host	Epidemiological Variable	Range of LWD (h)
Botrytis cinerea	strawberry flowers	disease incidence	6–32
Botrytis squamosa	onion leaves	number of lesions	6–32
Colletrotrichum acutation	strawberry fruit	disease incidence	3–40
Colletrotrichum coccodes	tomato fruit	severity	10–50
Diaporhe phaseolorum	soybean	disease incidence	2–140
Phakopsora pachyrizi	soybean	number of lesions	6–12
Phytophtora cactorum	strawberry fruit	infection	0.5–5
Puccinia arachidis	groundnut	lesion density	4–40
Puccinia recondita	wheat	infection hyphae	9–15
Puccinia striiformis	wheat	infection	3–6
Pyricularia grisea	ryegrass	number of lesions	6–48
Pyrenophora teres	barley	infection	3–24
Uromyces phaseoli	bean	number of pustules	4–25

Table 1.1. Wet period requirements for infection by several foliar pathogens (results published between 1985 and 1991) [14]. Reproduced with permission from Annual review of phytopathology. Adapted from Huber and Gillespie.

Infectious plant disease is defined as the plant's immune system response when inflicted by a pathogenic organism. Basic physiological or biochemical features including the plant's ability to reproduce, yield, or even maintain a normal structure are affected [12]. Ultimately, fungi are the most common causal agent of plant disease but require "free water" on the plant surface prior to infection [13]. Free water, in the form of rain, fog, or dew, provides an ideal environment for pathogenic microbe development. Huber and Gillespie conducted a literature review of work performed between 1985 and 1991 regarding the disease, crop affected and the range of wetness duration that is required

for the epidemiological variable indicated (Table 1.1) [14]. The duration of which is necessary for infection varies from a short period of time, as brief as half an hour for the infection of *Phytophthora cactorum* in strawberry fruit, to as long as 140 h for the development of *Diaporthe phaseolorum* in soybean.

'Volare'	
Wet Period (h)	Disease Index
4	1.67
5	2.22
6	3.56
24	4.00

'Magic Carousel'	
Wet Period (h)	Disease Index
4	0.33
8	0.89
12	1.22
24	3.67

Table 1.2. Disease index (0 to 5) 0 = no infections, 5 = all or nearly all petal tissue necrotic. Reproduced and adapted from D. Coyier [15]

As the wetness duration needed for infection varies, the severity of infection increases with longer leaf wetness periods. The severity of *Botrytis cinerea*, for example, on the 'Volare' Rose and 'Magic Carousel' Rose increases with longer wetness duration (Table 1.2) [15].

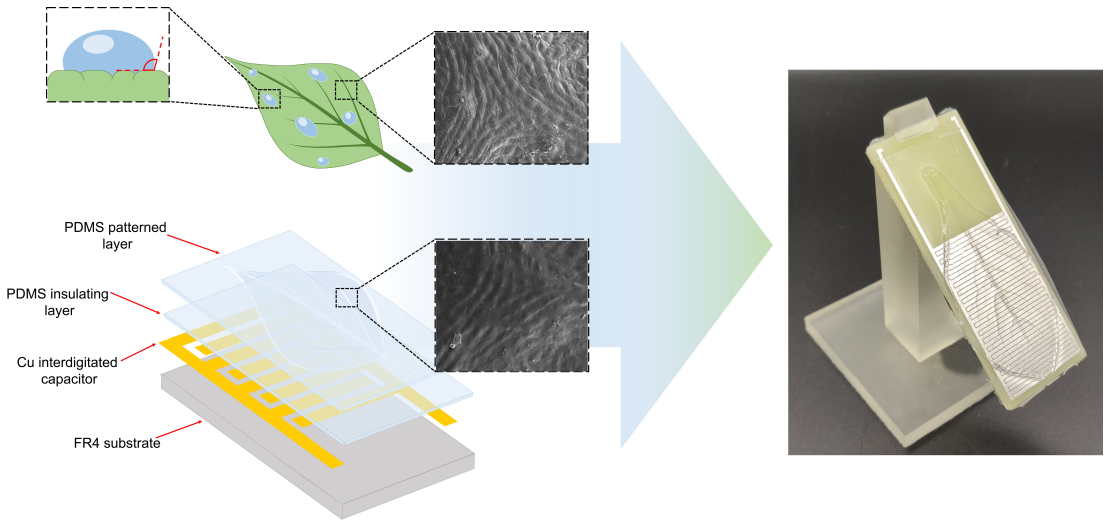

Figure 1.1. Schematic of bio-mimetic leaf wetness sensor with replica molded surface to accurately measure leaf wetness duration.

Monitoring environmental factors including humidity, temperature, rainfall and LWD are especially important. However, unlike environmental factors, LWD is not a standard meteorological measurement [16]. Moreoever, current sensors are unable mimic the surface of a leaf providing results that are not directly correlated with what truly occurs on a leaf surface. Accurately measuring leaf wetness duration, poses a significant challenge to correctly estimating the risk of fungal disease infections.To address the issues associated with commercially available LWS, we have fabricated a modified leaf wetness sensor by directly replicating the surface of leaves using polydimethylsiloxane replica molding soft lithography techniques (Fig. 1.1). In the following work, I demonstrated a LWS in which captures the complex leaf surface topography [17]. Therefore, by creating a bio-mimetic surface, the resulting wettability of the LWS closely matches that of the corresponding leaves.

Chapter 2

Background

Leaf wetness is a concern for the development of fungal pathogens for many plants. Hence, the measurement of the duration of time during which the leaves are wet is critical for plant disease management. In this section, I will address the different types of leaf wetness sensors (LWS) available, the capacitive sensor, the causes of leaf wetness, and engineered bio-mimetic surfaces.

2.1 The Leaf Wetness Sensor

Leaf wetness duration (LWD) is an important measurement in agricultural meteorology since it is a determining factor to pathogen infection and critical to the rate of plant disease development. To this end, agricultural communities have adopted leaf wetness sensors as a part of crop management systems to monitor the duration of leaf wetness resulting from dew, rainfall, or irrigation events. Over the duration of several decads, LWS have evolved from empirical methods to those based on electronics.

Sensors can be divided into three categories: static sensors, mechanical sensors, and electronic sensors.

Figure 2.1. (a) Duvdevani dew gauge, (b) De Wit leaf wetness recorder, (c) Davis Instruments resistive leaf wetness sensor, (d) METER Group Phytos 31

The static sensor contains no mechanical nor electronic components. A prime example of the static sensor is the Duvdevani dew gauge which operates based on

empirically examining dew formation on wooden blocks. The sensor is comprised of Wooden blocks that are painted red and placed outdoors, after sunset, at heights of 5, 25, 50, and 100 cm above the ground (Fig. 2.1(a)). Prior to sunrise, the dew formation of the painted block is then visually compared to a series of photographs called the dew scale. The dew scale acts as a reference for growers to compare and estimate the amount of dew formed [18]. Like most static sensors, the Duvdevani dew gauge relies on visual observation to estimate the amount of dew formed overnight but is lacking as it unable to provide a quantitative value for measuring dew duration.

The production of mechanical sensors aimed to resolve some of the shortcomings to static sensors. The De Wit leaf Wetness recorder, for example, consists of a length of string to measure water content during rainfall or periods of high relative humidity (Fig. 2.1(b)). It uses a hemp string that lengthens when exposed to moisture. The expansion and contraction of the string causes an ink pen to mark the duration of wet periods on a rotating chart [18]. Unlike its predecessor, the mechanical sensor takes a quantitative approach to measuring LWD. However, the mechanical sensor is also without its severe limitations. Rainfall is a significant contributor to the formation of water on leaf surfaces but this type of sensor cannot be used in precipitation events and is subject to numerous failures [18].

The electronic leaf wetness instrument has become the predominant method to measuring LWD. At the moment, there are two commercially available electronic LWS consisting of the resistive LWS and the the capacitive LWS [6]. The resistance LWS is comprised of a printed grid, where the circuit is complete when water on the sensor

surface bridges interlocking electrodes (Fig. 2.1(c)). The electrical resistance drops as water accumulates. The resistive LWS is not without flaws as its inability to measure small droplets and vulnerability to harsh environments make it unreliable. In contrast, the capacitive LWS is sensitive to sub-milligram levels of water condensing on the surface and is resilient to the harsh natural environment due to its insulated electrodes (Fig. 2.1(d)) [19]. The sensor functions by measuring a change in the capacitance seen at its insulated surface which then yields an output signal that changes according to its surface wetness. For its reliability, the capacitive LWS has become the gold-standard to LWS, but there are several limitations that need to be addressed. The capacitive LWS reflects only wetness on a particular surface of moderate wettability and is unable to effectively represent wetness of leaves of actual plants which vary tremendously [20]. In this work, I aim to take advantage of the capacitive LWS's strengths, but also remedy some of its short comings by modifying to surface to mimic the surfaces of actual plant leaves.

2.2 The Capacitive Sensor

Applications to capacitive sensing include the measurement or detection of humidity, position, fluid level, proximity, and acceleration [21]. Today, its most prominent use can be found in the touch screens of mobile devices and laptops. Human interaction such as a finger, ear, or hand elicits a capacitive change to the sensor element within the touch screen. This is often termed "capacitive touch" or "proximity," but sensing

is not limited to human interaction. In fact, other objects such as water droplets can change the capacitance seen at the sensor.

2.2.1 Capacitive Sensing Working Principle

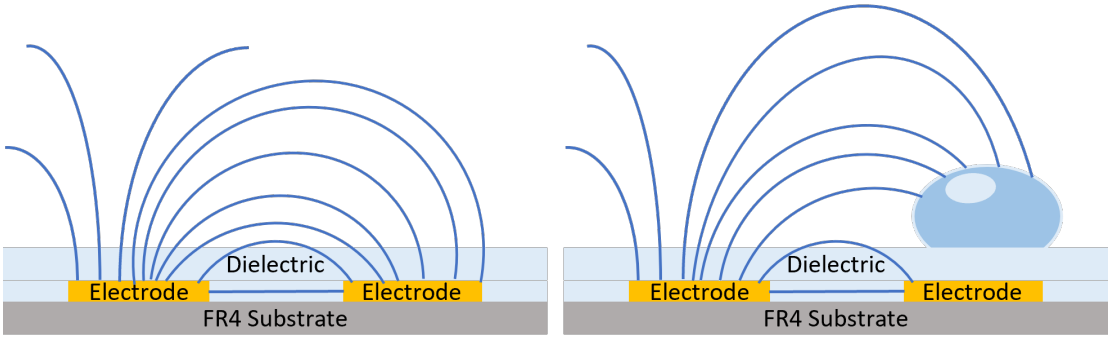

Figure 2.2. Water droplet interaction with the capacitor's electric field.

Capacitance is defined as a measure of an object's ability to store electric charge. If close enough together, any two conductive materials which are separated by a dielectric will exhibit capacitance [22]. Capacitors are typically designed to have a fixed value determined by the area of the two conductive plates, the distance between the plates, and the dielectric constant of the material between the plates. Altering the physical dimensions of the capacitor is not viable but, instead, the capacitance can be altered by "changing" the dielectric constant. Because a water droplet has much greater dielectric value than air, its interaction with the capacitor's electric field represents an overall increase its dielectric constant and thus an increase in its capacitance (Fig. 2.2) [22].

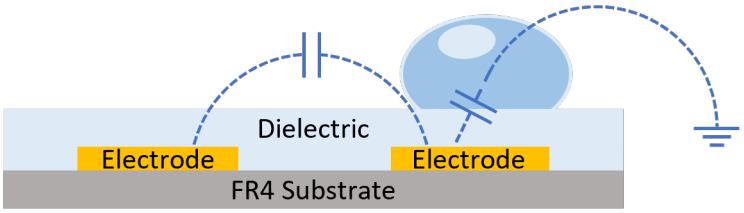

Figure 2.3. Equivalent circuit of droplet interaction with sensor.

The formation of a water droplet affects the overall dielectric constant seen at the surface of the sensor and therefore alters the overall capacitance. However, it must also be considered that the droplet acts as an additional capacitor in this system due to its inherent conductivity. The new capacitor formed by the water droplet is effectively in parallel with the existing PCB capacitor and, therefore, increases the system's overall capacitance (Fig. 2.3). Note that the water droplet itself is not electrically connected to the electrodes and is not in parallel in a circuit-analysis sense.

Two mechanisms are involved when a water droplet is formed on the surface of the capacitive sensor. First, because of the droplet's greater dielectric constant, its interaction with the capacitor's electric field produces an increase in capacitance. Simultaneously, the droplet's inherent conductivity forms a second capacitor in parallel with the PCB capacitor further increasing the overall capacitance of the system. We can see that both mechanisms govern the interaction between droplet and sensor but other factors such as the configuration of the capacitive sensing system also determines its effectiveness.

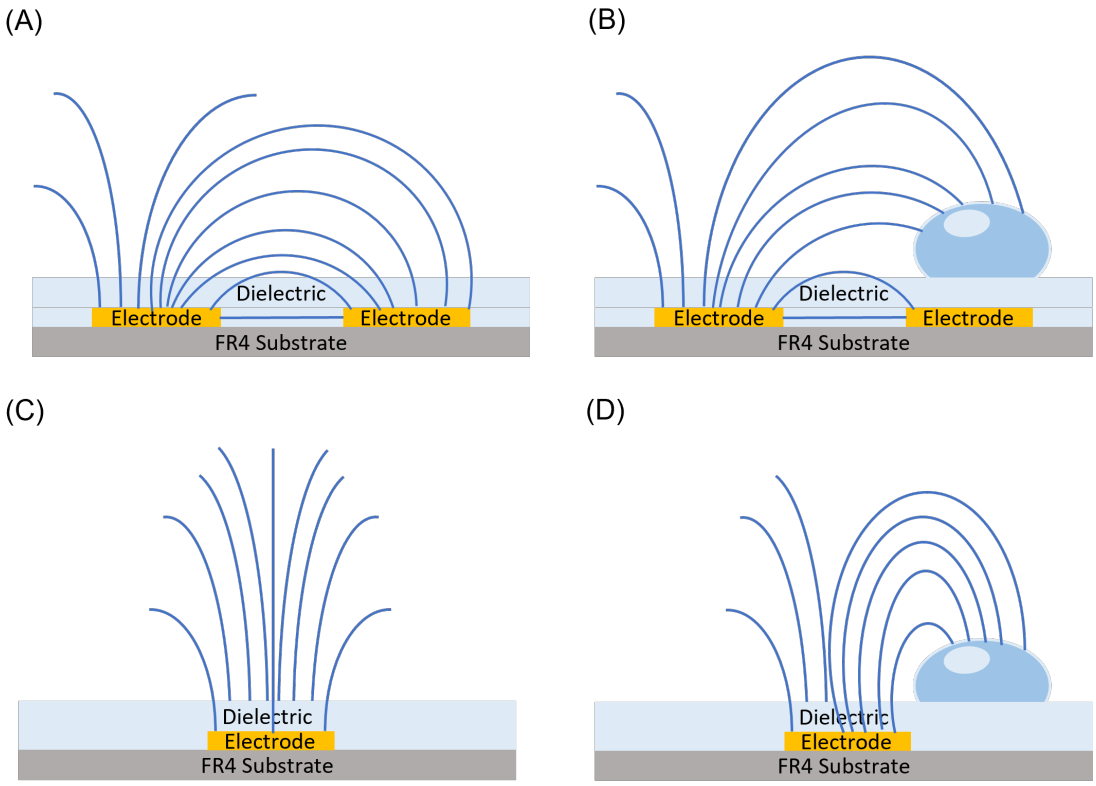

Figure 2.4. (a) Electric Field propagation of mutual-capacitance system (b) with water droplet. (c) Electric Field propagation of self-capacitance system (d) with water droplet.

Capacitive sensors fall into two types of categories: mutual capacitance and self-capacitance (Fig. 2.4). The operational principle of a self-capacitance sensor relies on measuring changes in capacitance with respect to earth ground. In a parallel-plate capacitor model, the electrode defines one plate of the capacitor while the other plate represents ground. In comparison, rather than have a single plate act as an electrode, mutual capacitance utilizes both plates to behave as electrodes [22]. Mutual capacitance electrodes consist of two separate electrode structures: the transmit electrode (Tx) and the receive electrode (Rx). The mutual capacitance formed between the Tx and Rx

form an electric field and, when disturbed by an object like a finger or water droplet, results in a change in capacitance [22].

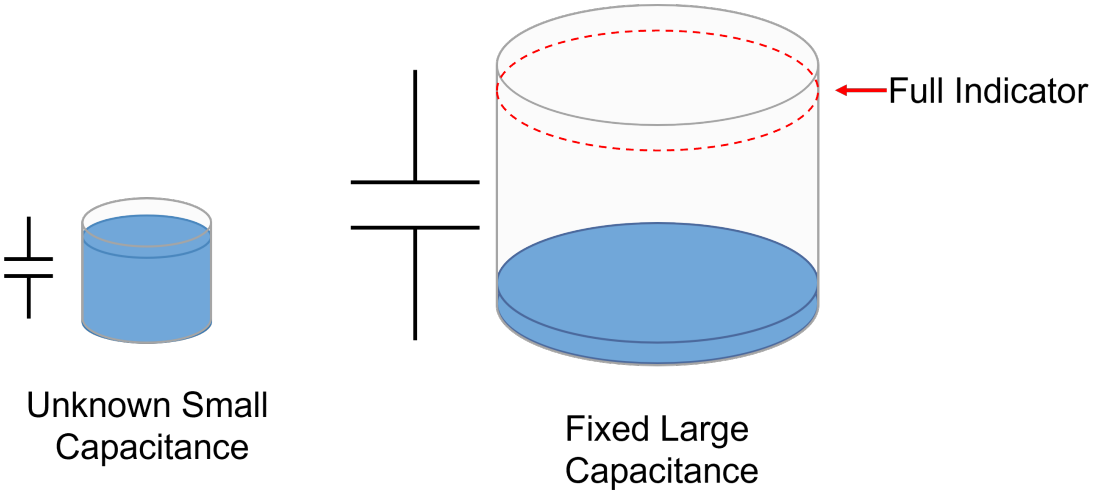

Figure 2.5. Working principle of charge transfer method to capacitance measurement.

Much of the capacitive sensor is dependent on the charge transfer method as an effective means to measure a change in capacitance based upon a fixed capacitance. In principle, the sensing circuit consists of two capacitors: a relatively large capacitor (C_L) of known fixed value and a variable capacitor(C_V) that is smaller than C_L . Charge transfer method operates by having C_V charged in which it is then transferred into C_L (Fig. 2.5). The capacitance of C_V is then determined based on the number of times it takes to fill C_L. Subsequently, if the number of times it takes to fill C_L changes, it indicates that the capacitance of C_V has altered [22]. It is this change in C_V that is measured and indicates if the surface of the capacitive sensor has been influenced.

2.2.2 Optimization of Capacitive Sensor Design

The working principle of the capacitive LWS is based on the fringing electric fields formed from the interdigital electrodes. The fringe electric field extends from the electrodes, out of the printed circuit board (PCB), where electrical environment changes from the formation of water droplets, result in an increase in capacitance. The performance of the sensor is determined by the penetration depth of its fringing field and its sensitivity which, in turn, are dependent on the geometry and material properties of the sensor. Consequently, there is a design tradeoff between the sensor's sensitivity and its penetration depth. Increasing the gap space between electrodes yields a greater penetration depth of the fringing field but also results in a loss in sensitivity [23, 24]. Conversely, decreasing the gap space increases the sensor's sensitivity but in-trade loses penetration depth. The primary goal of the capacitive sensor design is to achieve an optimum balance between these two factors [23].

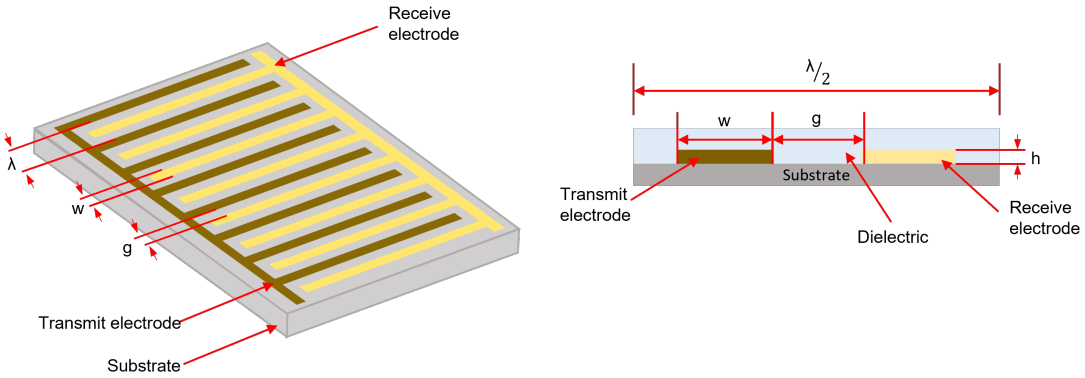

Figure 2.6. Perspective view and cross section of interdigital sensor.

Geometrical parameters including the width of the electrode digits (w), thickness of each electrode digit (h), number of electrode digits (N), and the gap size between them (g), are factors affecting the penetration depth of the fringing field and sensitivity of the sensor. In particular, the digit width-to-gap ratio, w/g, and the number of digits are key. A perspective view of the interdigital sensor is shown in Fig. 2.6.

2.3 Leaf Wettability

Leaf wettability can be described as the leaf's surface's affinity to water and varies based on the chemical composition and structure of leaf surfaces of the plant species. In a natural environment, leaf surfaces are frequently wetted by dewfall, precipitation, and irrigation events but depending on the tissue hygroscopicity, wettability can consist of individual drops or nanometer-thin water films [25]. In order to quantify leaf wettability, researchers use the contact angle (θ) of water on leaves measured at the gas, solid, and liquid interface as an index for surface wettability. Contact angles

between leaf surfaces and water droplets range from 0°to 180°. The variation across physical and chemical properties of leaf surfaces between species accounts to the different contact angles of leaves. These surface properties include chemical factors such as the content and microstructure of the epidermal wax and physical factors that consist of the number, size and pattern of trichomes, stomatal density, the shape of epidermal cells, and leaf water status [5, 6]. The wettability of leaves are categorized in the following way: "super-hydrophilic" if $\theta < 40°$, "highly wettable" if $\theta < 90°$, "wettable" if $\theta < 110°$, "non-wettable" if $\theta < 130°$, "highly non-wettable" if $\theta < 150°$, and "super-hydrophobic" if $\theta > 150°$ [6].

2.3.1 Criteria and measurement of leaf wettability

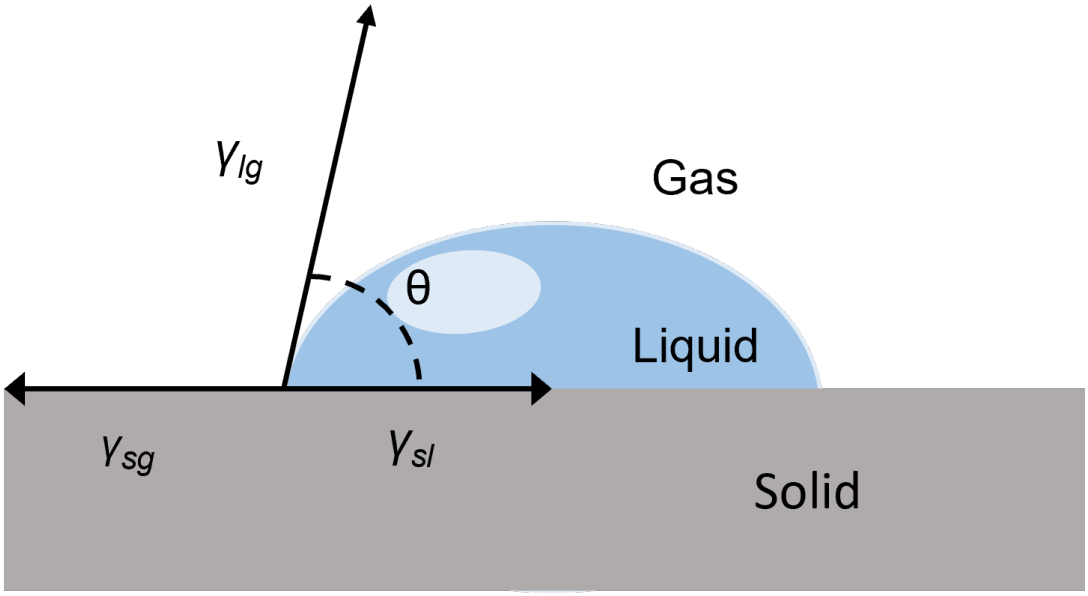

Figure 2.7. Young's modulus diagram of wetting of a solid surface with water, with air as the surrounding medium.

The extent of which a surface becomes wet is determined by the contact angle which is formed at the three-phase boundary where the liquid, gas, and solid intersect. The three free energies involved in this system consist of the solid-gas/vapor intersect (γ_{sg}), liquid-gas/vapor intersect (γ_{lg}), and solid-liquid/vapor intersect (γ_{sl}). The balance of the following forces of a water droplet on a smooth flat surface is explained by Young's equation [26]:

$$cos\theta_{smooth} = \frac{(y_{sg} - y_{sl})}{y_{lg}} \tag{2.1}$$

The contact angle given from Young's equation provides information regarding the interaction energy between the leaf surface and water droplet (Fig. 2.7) [27]. When $\gamma_{lg} = \gamma_{sl}$, the water droplet forms a contact angle of 90°. When $y_{sv} - y_{sl} \geq y_{sv}$, $\theta = 0$ and the water droplet completely spreads on the leaf surface. The contact angles between water droplets and the leaf surface are greater than 90°when $y_{sv} - y_{sl} < 0$. It is important to recognize that Young's equation is only applicable to ideal surfaces. Yet, leaf surfaces are rarely smooth due to three dimensional structures like the epidermis and cuticle structures. The presence of epicuticular waxes and trichomes also influences its roughness [7].

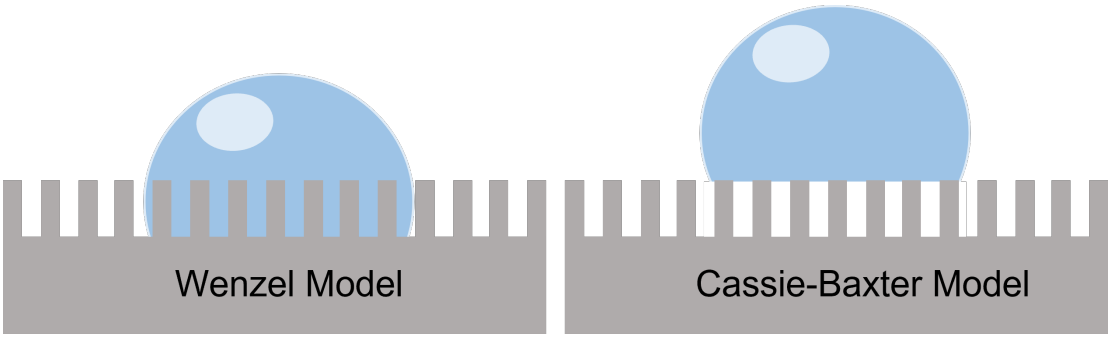

Figure 2.8. Diagram of Wenzel model and Cassie-Baxter model

To account for the contact angle formed on rough surfaces, Wenzel modified Young's equation by adding a roughness factor (r) as follows [28]:

$$cos\theta_{smooth} = cos\theta_{rough} = rcos\theta_{smooth} \tag{2.2}$$

The roughness factor is defined as the ratio of actual contact area of the leaf surface to the projected area of leaf surface that the droplet contacts [28]. While Wenzel's equation can account for surface roughness, the equation can only be applied to a homogeneous surface. Consequently, most leaf surfaces are heterogeneous and hence contact angle hysteresis occurs.

Contact angle hysteresis is defined as the difference between the contact angle of the advancing edge of a liquid drop, θ_a, and the contact angle of the receding edge of a liquid drop, θ_b. To account for a heterogeneous surface, a more complex model known as the Cassie-Baxter equation is required to measure how the apparent contact angle changes when various materials are involved [29]. For a surface with a two-component

surface, the Cassie-Baxter equation is expressed as:

$$cos\theta_c = f_1 cos\theta_1 + f_2 cos\theta_2 \tag{2.3}$$

In the Cassie-Baxter model, f represents the fraction of leaf surface area with a contact angle of θ. A surface in which incorporates patches of air and liquid on the leaf surface is a prime example. Due to the presence of small air pockets under the droplet in the Cassie-Baxter wetting scheme, the water droplet has less physical contact with the surface and a small contact angle hysteresis [29].

2.3.2 Bio-mimetic Surface Engineering

Bio-mimetic surface engineering can be interpreted as the adaptation of biological surface features on otherwise man-made materials. The addition of pattern or the control of chemical properties of a surface, may provide beneficial properties such as an induced wetting state and an enhanced interaction of materials with the environment. The lotus flower (Nelumbro nucifera) has become a popular example for artificial biologically inspired materials due to its super-hydrophobicity and self-cleaning property found on its leaves [30].

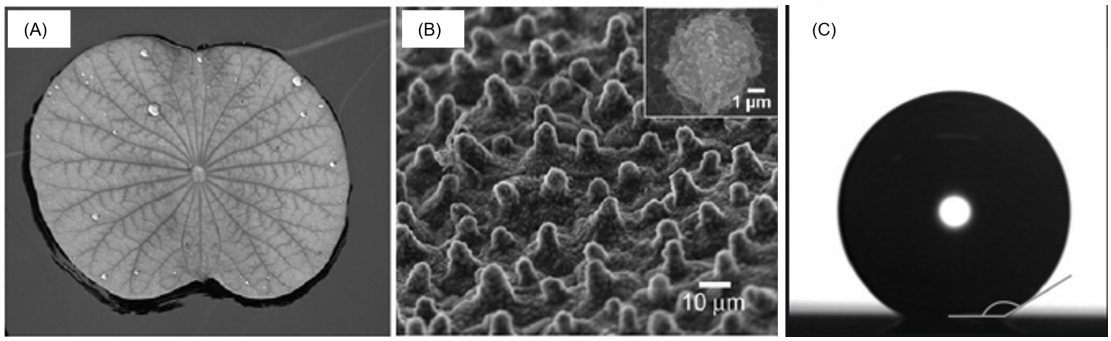

Figure 2.9. (a) A photo of a lotus leaf on the water. An ESEM image of the lotus surface.(b) The inset is a magnified image of the papilla structure.(c) Contact angle of lotus leaf. Reproduced with permission from the Royal Academy of Chemistry [30].

The lotus flower has a distinctive self-cleaning mechanism known as the "lotus effect." Its super-hydrophobic surface causes water droplets to bead up and roll off while collecting contaminants from its surface. This phenomenon is a result of micro-scale papillae covered with nano-scale wax crystals (Fig. 2.9). The heterogenous surface along with its ability to tilt or vibrate creates a self-cleaning surface promoting protection against fungal pathogen and aiding photosynthesis activity [30].

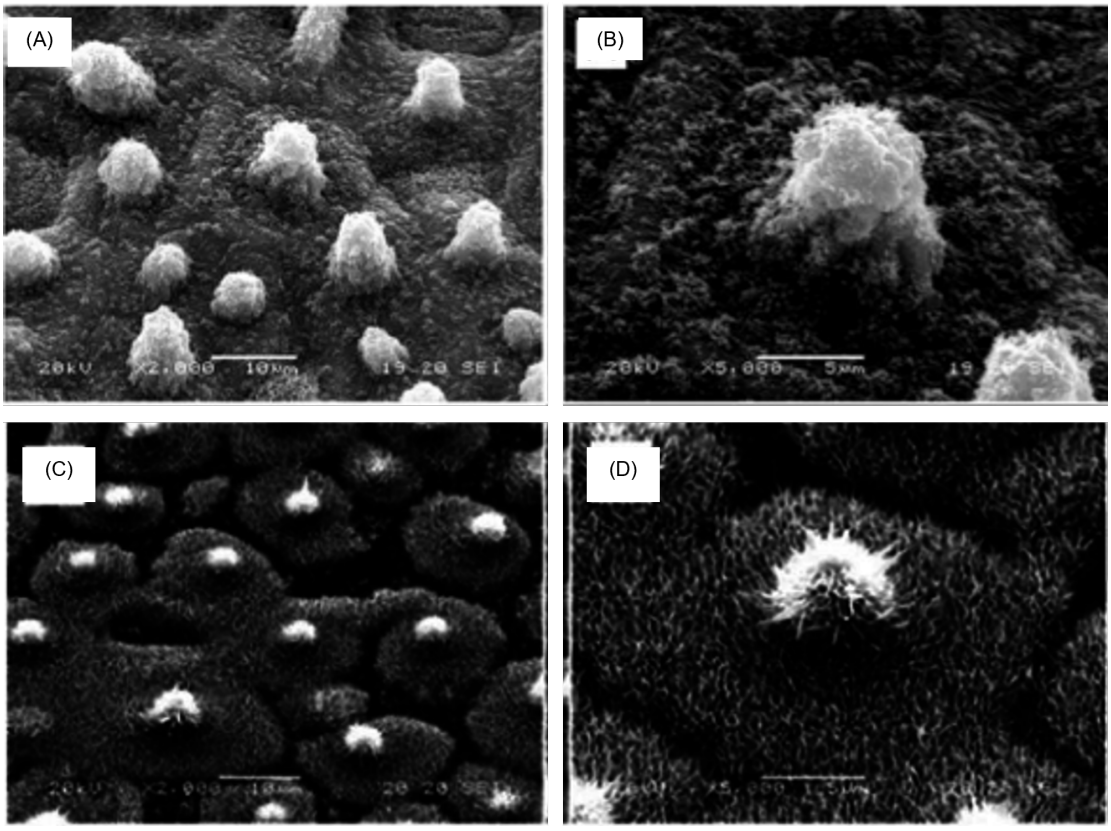

Figure 2.10. (a, b)SEM images of fresh lotus leaf surface composed of micro/nano scale binary structures. Typical SEM top-view and cross-section images of the as-prepared lotus-leaf-like hierarchical ZnO surfaces obtained (c, d). eproduced with permission from the Royal Academy of Chemistry [32].

Because the lotus leaf has become a popular subject for bio-inspiration, there have been numerous studies involving different methods to synthesize lotus-leaf-like surfaces. Lee et al. demonstrated a mass-production fabrication method involving nickel-mold making via electroforming which is then followed by a replication step via UV-nanoimprint lithography [31]. In addition, Dai et al. combined a sol-gel technique, soft lithography, and hydrothermal treatments to imprint microscale pillar structures from a PDMS mold directly into a ZnO sol film (Fig. 2.10) [32]. Similarly, mimicry

of hydrophilic leaf surfaces have also been reported. Kim et al. uses soft lithography in combination with polycaprolactone (PCL) and polyurethane acrylate (PUA) to fabricate surfaces that mimic the hydrophilic property of the common camellia (Camellia japonica) [33].

Chapter 3

Biomimetic Leaf Wetness Sensor Design, Fabrication, and Characterization

The objective of this work was to fabricate a modified bio-mimetic LWS using a simple double-casting method involving polydimethylsiloxane (PDMS) replica molding soft lithography techniques. In this section, I will discuss the design and testing of two components: the PDMS leaf replica and the capacitive LWS. I then verify surface replication and discuss capacitance measurement results.

3.1 Leaf Replica Fabrication and Assembly

Much of the internal factors that affect leaf wettability are owed to the microstructures found on its surface. It was important that during the leaf surface replication process, that details from its surface topography were retained to the utmost fidelity. The thickness of the patterned layer was also considered. One of the limita-

tions to the capacitive sensor is the penetration depth of its fringing fields at the sacrifice of sensitivity. Therefore, another goal was to design a fabrication process that yields a thin-enough layer to enable adequate sensor penetration with optimal sensitivity.

3.2 Template Mold and Fabrication

The process of creating the template is an easy and versatile method that is widely used to obtain bio-mimetic surfaces. The typical method involves a template with desired surface properties and pressing it on a soft polymer surface to copy its morphological features [32].

The casting process used polydimethylsiloxane (PDMS), an elastomer widely used for casting due to its low shrinkage properties during cure, excellent elasticity, and ability to replicate features at nanoscale resolution [34, 35]. In addition, PDMS is also ideal due to its water contact angle of 105° [36]. Because the controlled wetness properties of engineered surfaces are dependent on the natural properties of the material used to replicate the surface of leaves, I felt that the innate contact angle of PDMS acts as an optimal compromise between hydrophilic and hydrophobic [32]. Typically, when PDMS is prepared, a manufacturer-recommended 10:1 weight ratio between monomer and crosslinker is performed. However, for this process, it was important that I create a hard/soft dynamic between casting material and template to retain detail across surface-pattern transfer [37, 38]. To form this dynamic relationship, the ratio was adjusted to 20:1 to increase the disparity in stiffness between casting material and template [38, 39].

In choosing the casting polymer, the next step in the process was to design a casting method to form the leaf template. Leaves were prepared by first removing from plants, rinsed under running water for 1 min, and dried with nitrogen gas. Within the same day, the leaf was attached to a disposable Petri dish using double-sided Kapton tape. PDMS (20:1 weight ratio) was poured into the Petri dish containing the leaf and placed into the vacuum desiccator for 30 min to remove any further bubbles formed during the pouring process. Manufacturer protocol suggests curing PDMS in an oven at 60°C for 48 h, but at this temperature I observed that the leaf had lost much of its physical integrity due to the excessive heat. To remedy this issue, PDMS was cured instead in ambient air for 72 h. Once fully cured, the PDMS negative template was cut using a box cutter and peeled from leaf.

Following fabrication of the negative PDMS template mold, the next step was to form the positive PDMS replica. This process underwent two revisions. The first strategy was a protocol that involved a simple double casting method through plasma treatment followed by ethanol treatment to release a thin layer of patterned PDMS. The plasma treatment oxidizes the surface of the mold, showing an increase in the concentration of hydroxyl functional groups. Subsequent exposure of ethanol prevents adherence of the PDMS replica once cured [40]. Following surface passivation, I poured uncured PDMS into the template mold and excess elastomer was scraped away using a blade. The template along with the uncured PDMS was then cured in an oven at a temperature of 60°C for 48 h. Once fully cured, the positive replica layer was peeled away from the template mold to be bonded to the PCB sensor and act as a bio-mimetic

surface (Figure 3.1).

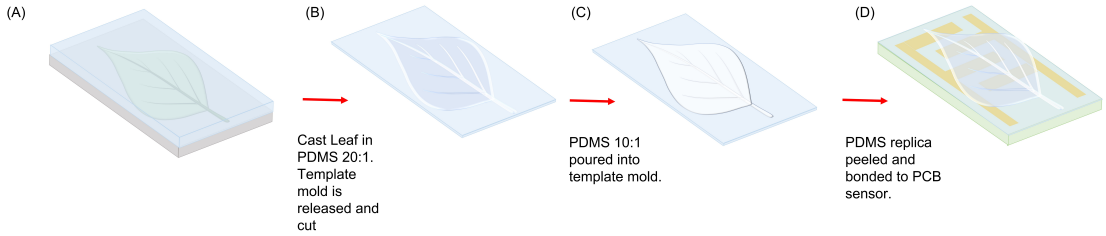

Figure 3.1. Initial strategy for replication of leaf surface onto capacitive sensor. The leaf of interest is mounted to a Petri dish using double-sided Kapton tape. (a) PDMS (20:1 weight ratio) is poured over the leaf and cured at room temperature. (b) The template mold is cut and peeled from the Petri dish. (c) PDMS (10:1 weight ratio) is poured into template mold and cured for 72 h at 60°C. (d) PDMS replica layer is peeled away from template mold and bonded to capacitive sensor.

However, upon use, this thin layer fabrication strategy suffered from various shortcomings. The two-step surface treatment was only able to prevent adhesion to a limited extent. I was able to separate the mold and replica but, because the replica layer was so thin and some adherence was still present, tearing occurred (Fig. 3.2a). The residual adherence was most likely due to the remaining uncrosslinked molecules and polar oxygenated species that was not fully leached by ethanol. While a thicker layer of PDMS would resolve the issue of tearing, an increase in the thickness of the replica layer would significantly limit the sensitivity of the sensor. Although, regardless if the replica-release method was successful, microscope imaging revealed that the layer was too thick at 380 µm to permit fringe field penetration (Fig. 3.2b).

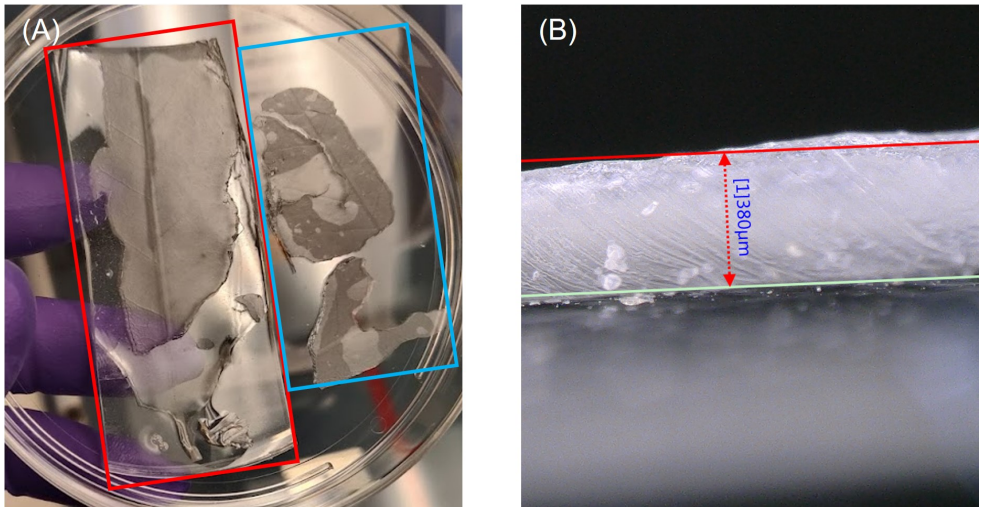

Figure 3.2. (a) Template mold highlighted in red and torn PDMS replica layer highlighted in blue. (b) Thickness of PDMS replica layer.

From flaws observed from the initial fabrication strategy, I had to address two issues: first, the use of ethanol as a passivation agent was not effective and, second, the current method of peeling away the replica layer was not viable if I was attempting to create a layer less than 380 µm thick. A new method had to be devised.

The second revision to my strategy still involved a double-casting method, but, rather than attempt to peel away and bond a thin patterned layer of PDMS, I instead used the negative template mold to act as a stamp and imprint the PCB sensor with the leaf pattern. To achieve this, I used a procedure called spin coating. Spin coating is a procedure used to deposit uniform thin films onto flat substrates, and, depending on the speed at which the material coating is subject to, the thickness of the film can be controlled. A 25 µm layer of PDMS (10:1 weight ratio) was first deposited onto the sensor by spin coating at 1000 rpm for 10 min and cured in an oven for 48 h. This first

layer acted as an insulating layer to protect the electrodes from corrosion.

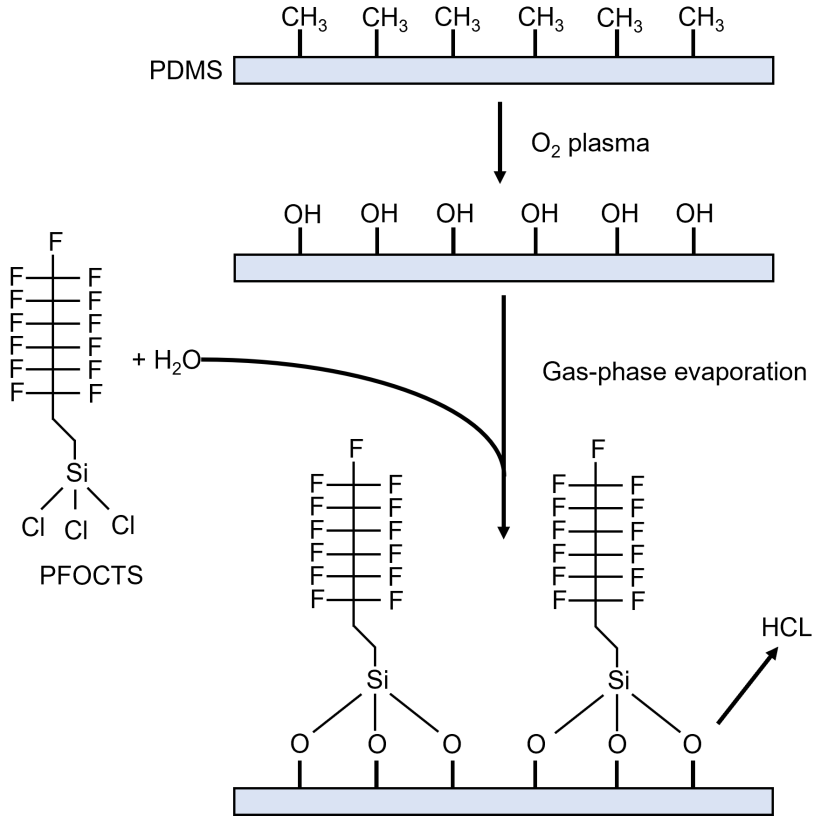

Figure 3.3. Schematic illustration of PDMS surface modification by PFOCTS.

To ensure the template mold did not adhere to the PCB sensor during pattern transfer, the template mold was treated with trichloro(1H,1H,2H,2H-perfluorooctyl) silane (PFOCTS) (97% Sigma Aldrich, USA). This chemical is commonly used as a self-assembled monolayer (SAM) on a mold as an anti-sticking agent for nanoimprint and has also been applied to PDMS to enable double casting [41–43]. PFOCTS's non-adhesive property is attributed to its several fluorine terminates [44].

A second layer of PDMS was spun on the PCB sensor but at 250 rpm for 60 s to yield a 200 µm layer. Before the PDMS was cured, the treated negative template

mold was then firmly pressed face-down into the coated PCB sensor. The assembly was placed in an oven to cure at a temperature of 60°C for 48 h. Once fully cured, the negative leaf replica mold was peeled from the PCB sensor exposing the patterned surface (Fig. 3.4). Profilometer measurements indicated that following double-casting procedures, the patterned PDMS layer had a maximum thickness of 180 µm.

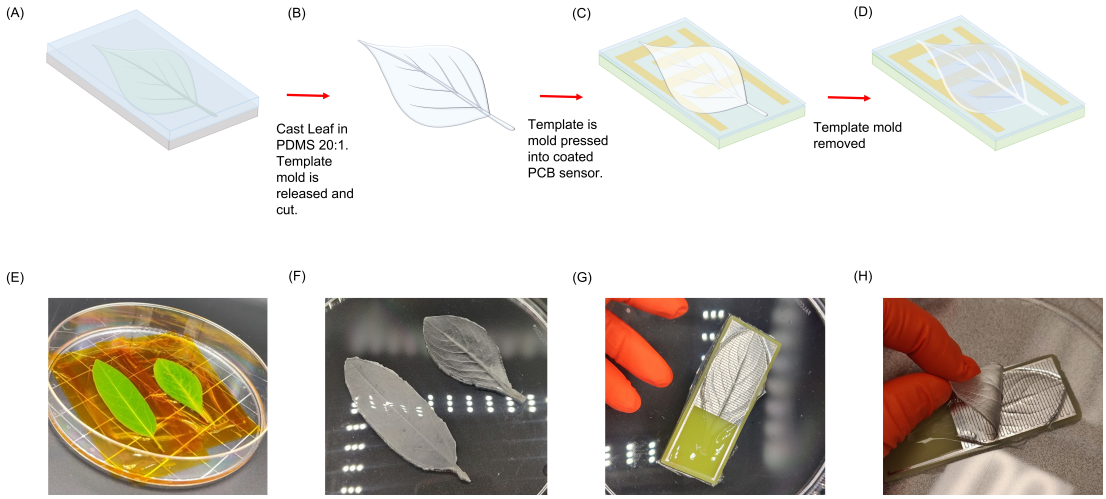

Figure 3.4. Working strategy for replication of leaf surface onto capacitive sensor. The leaf of interest is mounted to a Petri dish using double-sided Kapton tape. (a) PDMS (20:1 weight ratio) is poured over the leaf and cured at room temperature. (b) The template mold is cut and peeled from the Petri dish. (c) Template mold is then pressed face-down onto a PCB sensor that has been coated with uncured PDMS (10:1 weight ratio). PCB sensor is placed in an oven to cure at 60°C. (d)Template mold is peeled away from PCB sensor exposing the imprinted surface.

3.3 Printed Circuit Board Sensor Design

The capacitive sensor acts as the transducer in the bio-mimetic LWS. The fringe electric field extends from the electrodes, out of the printed circuit board (PCB), where electrical environment changes from the formation of water droplets, result in an

increase in capacitance. The performance of the sensor is determined by the penetration depth of its fringing field and its sensitivity. These two factors are dependent on the geometry and material properties of the sensor components.

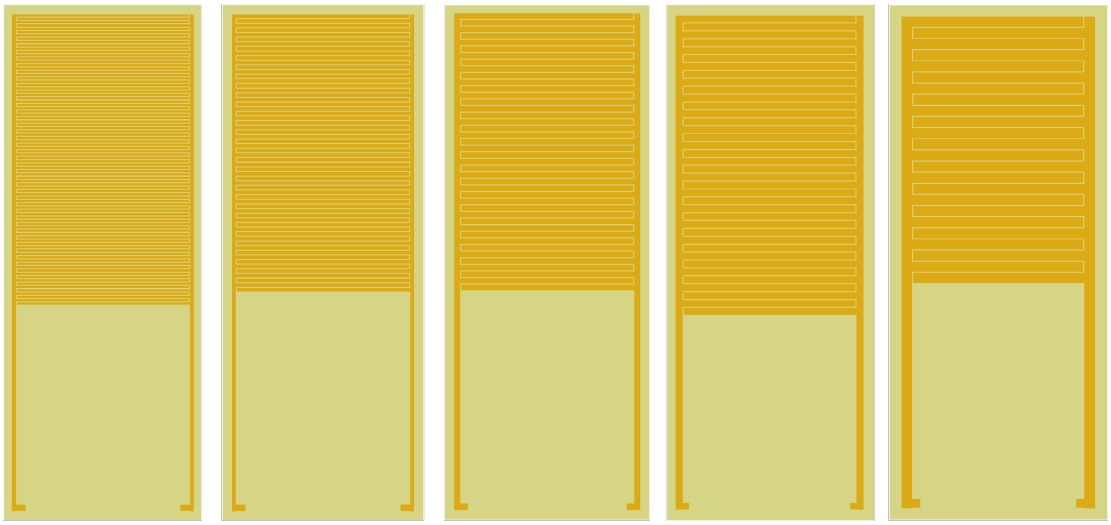

Figure 3.5. From left to right, PCB sensors with electrodes widths of 250 µm, 500 µm, 800 µm, 1000 µm, and 1500 µm. Each sensor caontined gap sizes of 250 µm.

Following double-casting procedures, the patterned PDMS layer had a maximum thickness of 180 µm. The goal during this portion of sensor design was to determine an optimal electrode width so as the fringing fields can penetrate the patterned layer of PDMS while still maintaining maximum sensitivity. To determine this parameter, PCB sensors of varying electrode widths were manufactured. Each sensor contained gap sizes of 250 µm but varied in electrodes widths of 250 µm, 500 µm, 800 µm, 1000 µm, and 1500 µm (Fig. 3.5). Designs were all constrained in a sensor head area of $20 \times 45\ mm^2$. In addition, an unmodified 180 µm layer of PDMS was deposited onto the sensor via spin coating to imitate the thickness of the leaf surface patterned layer. To test the limit

of detection for fringe field penetration, a sessile 0.5µl water droplet was placed on the surface for each sensor design and capacitance measurements were taken using an LCR meter (HANTEK 1832C). I found that among the sensor designs, an electrode width of 800 µm was able to detect a 0.8% change in capacitance with the 0.5 µl water droplet. A change in capacitance was not discernable with designs containing smaller electrode widths. This occurrence was most likely due to the fringe fields' inability to penetrate past 150 µm of PDMS. In contrast, while a change in capacitance was detectable with designs that included electrode widths of 1000 µm and 1500 µm, much of the signal was saturated with noise.

3.4 Surface Replica Verification

Three different bio-mimetic LWS were fabricated corresponding with a unique plant species. For this study, leaves of *Umbellularia californica* (California bay), *Platanus racemosa* (West Sycamore), and *Escallonia 'Iveyi'* (an Escallonia hybrid) were obtained from trees found on the University of California, Santa Cruz campus and were specifically chosen based on their diverse wettability. In addition, a LWS mimicking the PHYTOS 31 leaf wetness sensor (METER, USA) was fabricated and used as the basis for comparison against the other leaves.

Water contact angle measurements were taken for each leaf, the commercial sensor, and their replicas [45]. Contact angle measurements were obtained using a VHX-5000 Digital Microscope (Keyence, USA) and analyzed using Image J. Initial contact

angle measurements of the leaf replicas demonstrated that further surface modification was necessary to have the contact angles of the replicas and corresponding leaves match. To mediate this discrepancy, replicas were exposed to an oxygen plasma treatment to change the surface properties of the PDMS to a more hydrophilic state [46, 47].

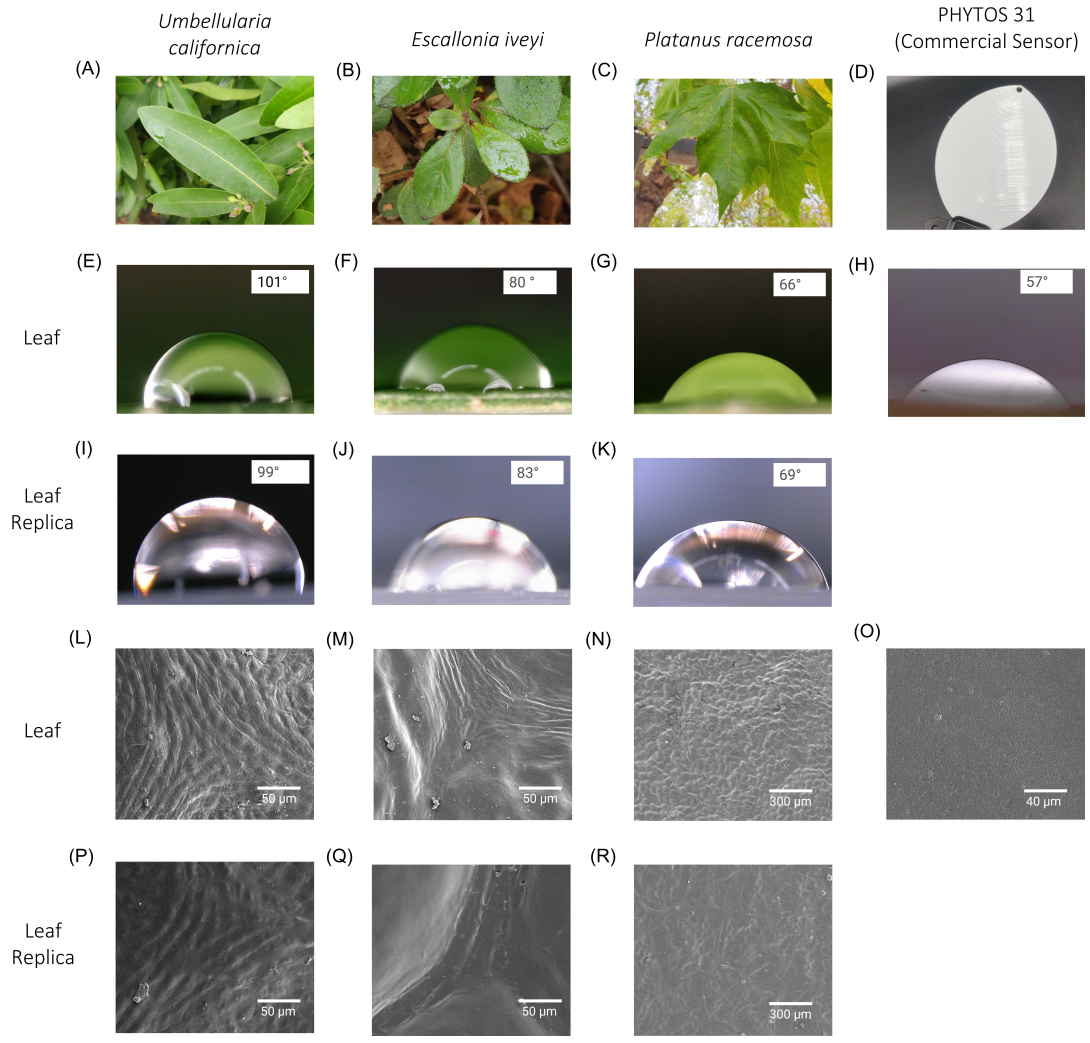

Figure 3.6. (a–d) Photographs of *Umbellularia californica*, *Platanus racemosa*, *Escallonia iveyi*, and commercial sensor. (e–h) Water contact angles of corresponding leaf samples and commercial sensor. (i–k) Water contact angles of PDMS leaf replicas. (l–o) SEM images of leaves and (p–r) their complementary PDMS replicas.

Based on the results from Fig. 3.6(e–r), the water contact angle measurements and SEM images verified that the replicas were able to capture the surface topography of each sample and closely match its wettability. The commercial sensor had a θ of 48° and is, therefore, termed "highly wettable". *P. racemosa* is categorized as "highly wettable" with a θ of 66°, *E. Iveyi* is "wettable" with a θ of 80°, and *U. californica* is "non-wettable" with a θ of 101°.

3.5 Humidity and Dew-Controlled Chamber

Dew is the moisture that forms as a product of condensation and occurs as the air surrounding an object becomes cold enough where it no longer has the capacity to hold water vapor. The water vapor in the air condenses causing small water droplets to form on the cold surface. The goal, following surface mimicry-verification, was to expose the bio-mimetic LWS to a similar dew-inducing environment and investigate its wetting properties. Factors, ranging from the relative humidity of the condensing environment to the degree of subcooling of the sample, contribute to the extent of condensation that occurs. As a result, controlling condensation in an experimental setup requires proper control of these factors. To test the the condensation behavior of the water droplets, I constructed a relative humidity and dew-controlled chamber (Fig. 3.7).

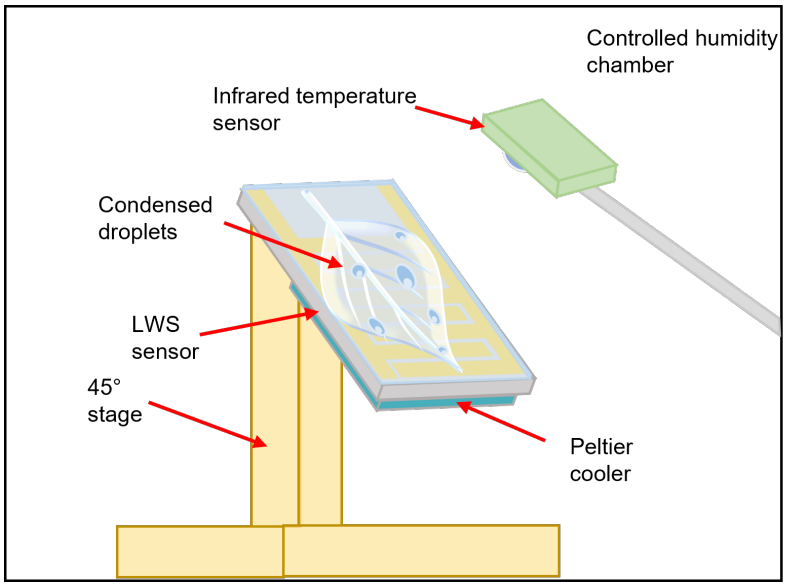

Figure 3.7. Diagram of humidity and condensation control chamber.

To reflect environmental conditions, the relative humidity of the chamber was maintained at 80% and the sensor surface kept at 45°F. The desired relative humidity was maintain by a means of spraying deonized water with an ultrasonic nebulizer where the exact humidity was monitored using a humidity sensor. In addition, the subcooling of the sensor surface was controlled by a Peltier-heat sink arrangement. The ultrasonic nebulizer and Peltier device were controlled by an ON/OFF trigger-driven mechanical relay connected to the Arduino environment [48]. However, temperature readings from an infrared temperature sensor recorded higher values compared to the Peltier set temperature owing to the thermal contact resistance of the 1.6mm sensor substrate [49–51]. To mediate this, an infrared camera was used on each LWS to monitor surface temperatures. Recordings of the fabricated LWS based on replicating the surface of its corresponding leaf species were performed. As a comparison, a LWS mimicking the

wettability of the commercial LWS was also placed within the chamber.

3.6 Wetting Measurements

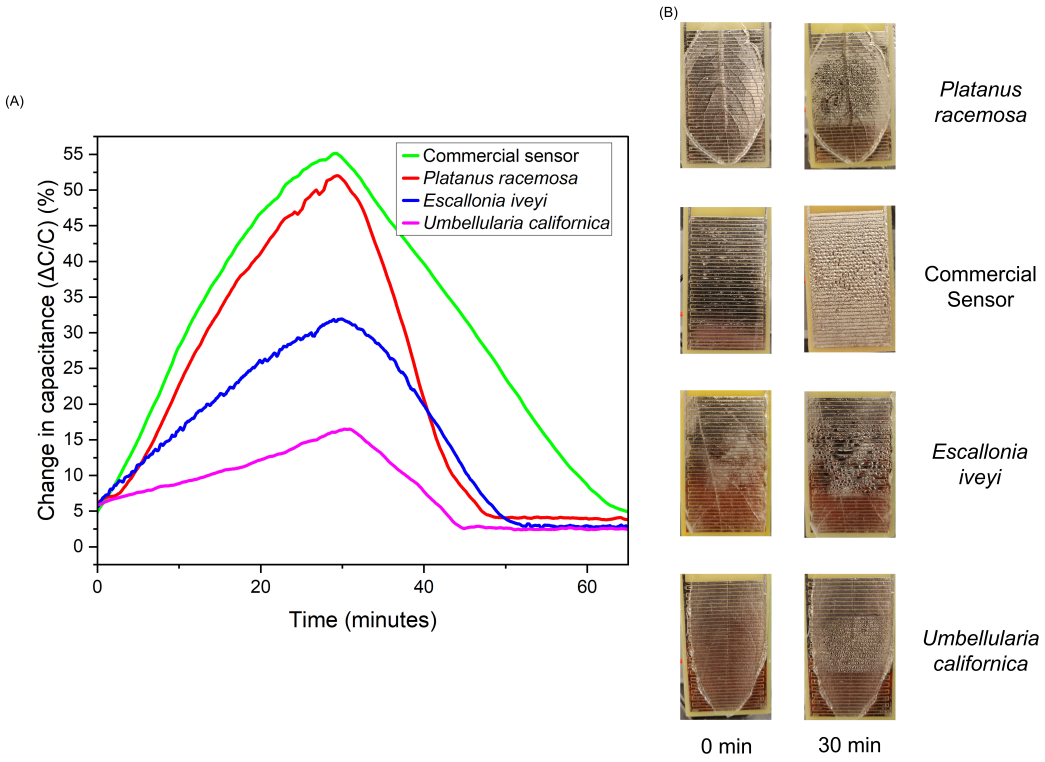

Figure 3.8. Response of replica LWSs measured via change in capacitance versus time. Once the commercial replica LWS reached full water surface saturation, dew chamber was deactivated and replica LWSs were allowed to dry. (a) The response of the LWSs were recorded and (b) corresponding photos were taken at 0 minutes and 30 minutes for each LWS.

Results shown in Fig. 3.8 confirm that the LWS's response is dependent on its wettability. At a 55% change in capacitance (ΔC), the surface of the sensor mimicking the commercial sensor was fully saturated with water. At this point, the *Platanus racemosa* replica LWS, which was the most hydrophilic leaf among the samples, exhibited

a similar response of the commercial replica LWS at 52% ΔC. Accordingly, the *E. Iveyi* yielded a 32% ΔC and the *U. californica* replica LWS displayed the smallest change at 9% ΔC. Once the commercial replica LWS reached full saturation, the humidity and dew-controlled chamber was shut off and the replica leaf sensors were allowed to dry in ambient air. The commercial replica LWS took roughly 30 min to reach full saturation, exhibiting a 55% ΔC. The commercial LWS replica exhibits a similar response to the *P. racemosa* replica LWS (52% ΔC) and, in principle demonstrates that it would be an adequate representation for *Platanus racemosa*. However, unlike the other replica LWS, the commercial replica LWS failed to accurately represent *E. Iveyi* and *U. californica* in terms of wettability. To reach 32% ΔC, it took the commercial replica LWS about 11 min while the *E. Iveyi* replica LWS requires 30 min. In a similar pattern, the commercial replica LWS requires only about 6 min to reach a similar saturation point to the *U. californica* replica LWS's . This discrepancy could potentially translate to severe misjudgments for LWD, and especially in the field, where water droplet formation could extend up to many hours [52]. Where other leaves like*E. Iveyi* and *U. californica* are more hydrophobic compared to *P. racemosa*, the commercial LWS may report full saturation after a certain period when the leaf is actually far from saturation.

Chapter 4

Conclusion

Accurately measuring LWD poses a significant challenge to correctly estimating the risk of fungal disease infections. While commercialized leaf sensors have demonstrated their ability to precisely measure surface water content in harsh environments, they are inadequate representations of actual leaves because they do not consider leaf wettability. Therefore, the purpose of this study was to establish the importance of leaf wettability as a parameter when designing LWS. The use of commercial LWS appears to be adequate for plants that have leaves with comparable leaf wetness properties. However, with species with hydrophobic or hydrophilic leaves, there is a great potential for error when determining LWD. The results points to the importance of using sensors with appropriate surface wettability when determining LWD and offers an easy method to fabricating a more representative LWS. However, while we were able to verify contrasting responses between the commercial replica LWS and other LWS, further verification is necessary.

4.1 Outlook

In this work, while I was able to demonstrate that leaf wettability as a parameter for LWS is critical, there are further limitations in this work that need to be addressed.

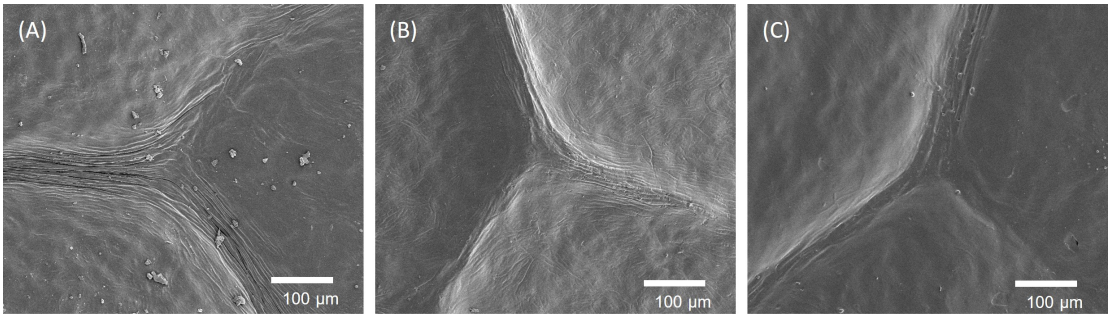

Figure 4.1. (a) SEM image of *Escallonia iveyi*. SEM image of template mold for *Escallonia iveyi*. SEM of image of PDMS replica for *Escallonia iveyi*.

With the double casting method, the leaf surface pattern is transferred twice: once from the leaf to the negative template mold, and again from the negative template mold to the positive replica. It is evident from Fig. 4.1 during the casting process there was some loss of morphology detail. The negative mold was able to effectively capture the micro-scale features of the plant leaf but, moving from negative template mold to positive replica, the loss is apparent. This shortcoming was most likely owing to the hard/soft dynamic between casting material and mold not being significant enough. A polymer with a high Young's modulus, like SU-8 photoresist, would be a better material to act as the positive replica mold [53]. SU-8's stiffer properties would yield a greater hard/soft dynamic and, accordingly, micro-structures can be better retained during casting.

Another limitation is the mismatch of rigidity between LWS and leaves. This limitation, in fact, is applicable to all electronic LWS as they are typically composed of hard materials. On the other hand, plant leaves typically flexible and will bend to allow excess water to travel down the leaf surface [54, 55]. Removing excess water from the leaf surface helps to prevent fungal growth. Fabricating the LWS on a flexible substrate may provide more representative data for specific crops [56].

4.2 Future Work

For this work, there are many opportunities to improve the sensor. Further optimization of the geometrical parameters of the interdigitated electrodes on the capacitive sensor can better its performance. Using a more rigid polymer like SU-8 to form the positive replica could better maintain the surface micro-structures during pattern transfer. Lastly, fabricating the sensor on a flexible substrate like PDMS could potentially produce more representative LWD data.

Though, more significantly, the next steps in this study are to perform field in-situ LWD measurements. Strawberries and beans are of particular interest because of their potential as profitable crops but are also recognized to be easily susceptible to disease development. Further work would see deployment of the bio-mimetic LWS in strawberry and bean fields.

Bibliography

[1] A. Sarkozi, "New standards to curb the global spread of plant pests and diseases," 2019.

[2] S. Kamal Dev, S. Vinod, S. Ravinder, and N. Harsh, "Control of chickpea blight disease caused by didymella rabiei by mixing resistance inducer and contact fungicide," *Crop Protection*, vol. 30, no. 11, pp. 1519–1522, 2011.

[3] J. A. Davidson and R. B. E. Kimber, "Integrated disease management of ascochyta blight in pulse crops," *European Journal of Plant Pathology*, vol. 119, no. 1, pp. 99–110, 2007.

[4] C. Yarwood, *Water and the infection process*. Academic Press New York, NY, 1978, vol. 5, pp. 141–173.

[5] H. Wang, H. Shi, and Y. Wang, "The wetting of leaf surfaces and its ecological significances," M. Aliofkhazraei, Ed., vol. Wetting and Wettability. IntechOpen, Conference Proceedings.

[6] T. Rowlandson, M. Gleason, P. Sentelhas, T. Gillespie, C. Thomas, and B. Horn-

buckle, "Reconsidering leaf wetness duration determination for plant disease management," *Plant Disease*, vol. 99, no. 3, pp. 310–319, 2015.

[7] K. Kim, S. Taylor, M. Gleason, and K. Koehler, "Model to enhance site-specific estimation of leaf wetness duration," *Plant disease*, vol. 86, no. 2, pp. 179–185, 2002.

[8] R. Magarey, J. Russo, and R. Seem, "Simulation of surface wetness with a water budget and energy balance approach," *Agricultural and forest meteorology*, vol. 139, no. 3-4, pp. 373–381, 2006.

[9] P. C. Sentelhas, A. Dalla Marta, S. Orlandini, E. A. Santos, T. J. Gillespie, and M. L. Gleason, "Suitability of relative humidity as an estimator of leaf wetness duration," *Agricultural and forest meteorology*, vol. 148, no. 3, pp. 392–400, 2008.

[10] P. C. Sentelhas, T. J. Gillespie, M. L. Gleason, J. E. B. Monteiro, J. R. M. Pezzopane, and M. J. Pedro Jr, "Evaluation of a penman–monteith approach to provide "reference" and crop canopy leaf wetness duration estimates," *Agricultural and Forest Meteorology*, vol. 141, no. 2-4, pp. 105–117, 2006.

[11] V. O. Montone, C. W. Fraisse, N. A. Peres, P. C. Sentelhas, M. Gleason, M. Ellis, and G. Schnabel, "Evaluation of leaf wetness duration models for operational use in strawberry disease-warning systems in four us states," *Int J Biometeorol*, vol. 60, no. 11, pp. 1761–1774, 2016, 1432-1254 Montone, Verona O Fraisse, Clyde W Peres, Natalia A Sentelhas, Paulo C Gleason, Mark Ellis, Michael Schnabel, Guido Journal

Article United States 2016/11/01 Int J Biometeorol. 2016 Nov;60(11):1761-1774. doi: 10.1007/s00484-016-1165-4. Epub 2016 May 14.

[12] O. C. Maloy, "Plant disease management," *The Plant Health Instructor*, 2005.

[13] S. D. Ellis, M. J. Boehm, and T. K. Mitchell, "Fungal and fungal-like diseases of plants," Conference Proceedings.

[14] L. Huber and T. J. Gillespie, "Modeling leaf wetness in relation to plant disease epidemiology," *Annual Review of Phytopathology*, vol. 30, no. 1, pp. 553–577, 1992.

[15] D. L. Coyier and M. K. Roane, *Compendium of rhododendron and azalea diseases*. Aps Press, 1986.

[16] A. Madeira, K. Kim, S. Taylor, and M. Gleason, "A simple cloud-based energy balance model to estimate dew," *Agricultural and Forest Meteorology*, vol. 111, no. 1, pp. 55–63, 2002.

[17] M. Sun, C. Luo, L. Xu, H. Ji, Q. Ouyang, D. Yu, and Y. Chen, "Artificial lotus leaf by nanocasting," *Langmuir*, vol. 21, no. 19, pp. 8978–8981, 2005, doi: 10.1021/la050316q.

[18] R. R. Getz, "Report on the measurement of leaf wetness," *World Meteorlogical Organizaiton*, p. 10, 1992.

[19] "Phytos 31 operator manual," Court Pullman, WA, 2021.

[20] "Lws dielectric leaf wetness sensor product manual," Logan, UT, 2018.

[21] M. Shadwani, S. Sachan, and P. Sachan, *Capacitive Sensing Its Applications*, 2018.

[22] "Capacitive sensing basics," 5/28/2020 2017.

[23] Y. Huang, Z. Zhan, and N. Bowler, "Optimization of the coplanar interdigital capacitive sensor," *AIP Conference Proceedings*, vol. 1806, no. 1, p. 110017, 2017.

[24] X. B. Li, S. D. Larson, A. S. Zyuzin, and A. V. Mamishev, "Design of multichannel fringing electric field sensors for imaging. part i. general design principles," in *Conference Record of the 2004 IEEE International Symposium on Electrical Insulation*, Conference Proceedings, pp. 406–409.

[25] O. Klemm, C. Milford, M. A. Sutton, G. Spindler, and E. M. Putten, "A climatology of leaf surface wetness," *Theoretical and Applied Climatology*, vol. 71, pp. 107–117, 2002.

[26] T. Young, "Iii. an essay on the cohesion of fluids," *Philosophical transactions of the royal society of London*, no. 95, pp. 65–87, 1805.

[27] B. H. P. Rosado and C. D. Holder, "The significance of leaf water repellency in ecohydrological research: a review," *Ecohydrology*, vol. 6, no. 1, pp. 150–161, 2013.

[28] R. N. Wenzel, "Resistance of solid surfaces to wetting by water," *Industrial Engineering Chemistry*, vol. 28, no. 8, pp. 988–994, 1936, doi: 10.1021/ie50320a024.

[29] A. Cassie and S. Baxter, "Wettability of porous surfaces," *Transactions of the Faraday society*, vol. 40, pp. 546–551, 1944.

[30] J. Zhang, J. Wang, Y. Zhao, L. Xu, X. Gao, Y. Zheng, and L. Jiang, "How does the leaf margin make the lotus surface dry as the lotus leaf floats on water?" *Soft Matter*, vol. 4, no. 11, pp. 2232–2237, 2008.

[31] S.-M. Lee and T. H. Kwon, "Mass-producible replication of highly hydrophobic surfaces from plant leaves," *Nanotechnology*, vol. 17, no. 13, pp. 3189–3196, 2006.

[32] D. Kim, W. Kim, S. Park, S. Kim, Y. Gwon, and J. Kim, "Leaf-inspired micro- and nanoengineered surfaces for controlled hydrophilic and hydrophobic properties," *Macromolecular Research*, vol. 28, no. 1, pp. 57–61, 2020.

[33] S. Dai, D. Zhang, Q. Shi, X. Han, S. Wang, and Z. Du, "Biomimetic fabrication and tunable wetting properties of three-dimensional hierarchical zno structures by combining soft lithography templated with lotus leaf and hydrothermal treatments," *CrystEngComm*, vol. 15, pp. 5417–5424, 2013.

[34] J. Friend and L. Yeo, "Fabrication of microfluidic devices using polydimethylsiloxane," *Biomicrofluidics*, vol. 4, no. 2, p. 026502, 2010, 20697575[pmid] PMC2917889[pmcid] 026502[PII].

[35] F. Hua, Y. Sun, A. Gaur, M. A. Meitl, L. Bilhaut, L. Rotkina, J. Wang, P. Geil, M. Shim, J. A. Rogers, and A. Shim, "Polymer imprint lithography with molecular-scale resolution," *Nano Letters*, vol. 4, no. 12, pp. 2467–2471, 2004, doi: 10.1021/nl048355u.

[36] A. Mata, A. J. Fleischman, and S. Roy, "Characterization of polydimethylsiloxane

(pdms) properties for biomedical micro/nanosystems," *Biomedical Microdevices*, vol. 7, no. 4, pp. 281–293, 2005.

[37] B. Kwon and J. Kim, "Importance of molds for nanoimprint lithography: Hard, soft, and hybrid molds," *Journal of Nanoscience*, vol. 2016, pp. 1–12, 2016.

[38] W. Wu, R. M. Guijt, Y. E. Silina, M. Koch, and A. Manz, "Plant leaves as templates for soft lithography," *RSC Advances*, vol. 6, no. 27, pp. 22 469–22 475, 2016.

[39] Z. Wang, A. A. Volinsky, and N. D. Gallant, "Crosslinking effect on polydimethylsiloxane elastic modulus measured by custom-built compression instrument," *Journal of Applied Polymer Science*, vol. 131, no. 22, 2014.

[40] K. Sung-Hwan, L. Seungjin, A. Dongchan, and P. Joong Yull, "Pdms double casting method enabled by plasma treatment and alcohol passivation," *Sensors and Actuators B: Chemical*, vol. 293, pp. 115–121, 2019.

[41] S. Onclin, B. J. Ravoo, and D. N. Reinhoudt, "Engineering silicon oxide surfaces using self-assembled monolayers," *Angewandte Chemie International Edition*, vol. 44, no. 39, pp. 6282–6304, 2005.

[42] M. Zhang, J. Wu, L. Wang, K. Xiao, and W. Wen, "A simple method for fabricating multi-layer pdms structures for 3d microfluidic chips," *Lab Chip*, vol. 10, no. 9, pp. 1199–203, 2010, zhang, Mengying Wu, Jinbo Wang, Limu Xiao, Kang Wen, Weijia Journal Article England 2010/04/15 Lab Chip. 2010 May 7;10(9):1199-203. doi: 10.1039/b923101c. Epub 2010 Feb 9.

[43] J.-K. Chen, F.-H. Ko, K.-F. Hsieh, C.-T. Chou, and F.-C. Chang, "Effect of fluoroalkyl substituents on the reactions of alkylchlorosilanes with mold surfaces for nanoimprint lithography," *Journal of Vacuum Science Technology B: Microelectronics and Nanometer Structures Processing, Measurement, and Phenomena*, vol. 22, no. 6, pp. 3233–3241, 2004.

[44] D. M. Lemal, "Perspective on fluorocarbon chemistry," *The Journal of Organic Chemistry*, vol. 69, no. 1, pp. 1–11, 2004, doi: 10.1021/jo0302556.

[45] D. J. Gomes, N. de Souza, and J. Silva, "Using a monocular optical microscope to assemble a wetting contact angle analyser," *Measurement*, vol. 46, p. 3623, 2013.

[46] T. Trantidou, Y. Elani, E. Parsons, and O. Ces, "Hydrophilic surface modification of pdms for droplet microfluidics using a simple, quick, and robust method via pva deposition," *Microsyst Nanoeng*, vol. 3, p. 16091, 2017, 2055-7434 Trantidou, Tatiana Elani, Yuval Parsons, Edward Ces, Oscar Journal Article 2017/04/24 Microsyst Nanoeng. 2017 Apr 24;3:16091. doi: 10.1038/micronano.2016.91. eCollection 2017.

[47] S. H. Tan, N. T. Nguyen, Y. C. Chua, and T. G. Kang, "Oxygen plasma treatment for reducing hydrophobicity of a sealed polydimethylsiloxane microchannel," *Biomicrofluidics*, vol. 4, no. 3, p. 32204, 2010, 1932-1058 Tan, Say Hwa Nguyen, Nam-Trung Chua, Yong Chin Kang, Tae Goo Journal Article 2010/11/04 Biomicrofluidics. 2010 Sep 30;4(3):32204. doi: 10.1063/1.3466882.

[48] R. Gupta, C. Das, A. Roy, R. Ganguly, and A. Datta, "Arduino based temperature and humidity control for condensation on wettability engineered surfaces," in *2018 Emerging Trends in Electronic Devices and Computational Techniques (EDCT)*. IEEE, 2018, pp. 1–6.

[49] A. Ghosh, S. Beaini, B. Zhang, R. Ganguly, and C. Megaridis, "Enhancing dropwise condensation through bioinspired wettability patterning," *Langmuir : the ACS journal of surfaces and colloids*, vol. 30, 2014.

[50] S. M. Yoon, T.-J. Ko, K. H. Oh, S. Nahm, and M.-W. Moon, "Water wetting observation on a superhydrophobic hairy plant leaf using environmental scanning electron microscopy," *Applied Microscopy*, vol. 46, no. 4, pp. 201–205, 2016.

[51] J. Trosseille, A. Mongruel, L. Royon, M.-G. Medici, and D. Beysens, "Roughness-enhanced collection of condensed droplets," *The European Physical Journal E*, vol. 42, 2019.

[52] P. C. Sentelhas, T. J. Gillespie, and E. A. Santos, "Leaf wetness duration measurement: comparison of cylindrical and flat plate sensors under different field conditions," *Int J Biometeorol*, vol. 51, no. 4, pp. 265–73, 2007, sentelhas, Paulo C Gillespie, Terry J Santos, Eduardo A Comparative Study Evaluation Study Journal Article United States 2006/11/25 Int J Biometeorol. 2007 Mar;51(4):265-73. doi: 10.1007/s00484-006-0070-7. Epub 2006 Nov 24.

[53] J. N. Patel, B. L. Gray, B. Kaminska, N.-C. Wu, and B. D. Gates, "Su-8-and

pdms-based hybrid fabrication technology for combination of permanently bonded flexible and rigid features on a single device," *Journal of Micromechanics and Microengineering*, vol. 23, no. 6, p. 065029, 2013.

[54] C. T. Ivey and N. DeSilva, "A test of the function of drip tips," *Biotropica*, pp. 188–191, 2001.

[55] J. M. Dean and A. P. Smith, "Behavioral and morphological adaptations of a tropical plant to high rainfall," *Biotropica*, pp. 152–154, 1978.

[56] K. S. Patle, R. Saini, A. Kumar, S. G. Surya, V. S. Palaparthy, and K. N. Salama, "Iot enabled, leaf wetness sensor on the flexible substrates for in-situ plant disease management," *IEEE Sensors Journal*, vol. 21, no. 17, pp. 19 481–19 491, 2021.

[57] D. L. Ahmad, R. H. Kanth, S. Parvaze, and D. S. S. Mahdi, "Experimental agrometeorology: A practical manual," in *Springer International Publishing*, Conference Proceedings.

[58] K. Aung, Y. Jiang, and S. Y. He, "The role of water in plant-microbe interactions," *Plant J*, vol. 93, no. 4, pp. 771–780, 2018, 1365-313x Aung, Kyaw Jiang, Yanjuan He, Sheng Yang K99 GM115766/GM/NIGMS NIH HHS/United States R00 GM115766/GM/NIGMS NIH HHS/United States R01 GM109928/GM/NIGMS NIH HHS/United States Journal Article Research Support, N.I.H., Extramural Research Support, Non-U.S. Gov't Review 2017/12/06 Plant J. 2018 Feb;93(4):771-780. doi: 10.1111/tpj.13795. Epub 2018 Jan 14.

[59] Y. He, S. Xiao, J. Wu, and H. Fang, "Influence of multiple factors on the wettability and surface free energy of leaf surface," *Applied Sciences*, vol. 9, no. 3, p. 593, 2019.

Appendix A

Supplementary Information

A.1 Printed Circuit Board Sensor Design

The PCB sensor interdigitated electrode design was printed on a 1.6mm thick fiberglass substrate and with the sensor head area constrained to a 20 × 45 mm2 area. Each electrode had a finger width of 1 mm and a gap space of 250 µm. The PCB electrode side is covered with a 25 m protective coating of PDMS (10:1 weight ratio), by spin coating at 1000 rpm for 10 min. The coated PCB sensor was cured in an oven at a temperature of 60°C for 48h.

A.2 Leaf Replica Fabrication

To create the negative mold, leaves were first removed from plants, rinsed under running water for one minute, and dried with nitrogen gas. Within the same day, the leaf was attached to a disposable Petri dish using double-sided Kapton tape. PDMS

(SYLGARD 184; Dow Corning, USA) was prepared by mixing the PDMS prepolymer and cross linker in a 20:1 weight ratio and degassed for 1 h in a vacuum desiccator to remove air bubbles. The 20:1 ratio PDMS was poured into the Petri dish containing the leaf and placed back into the vacuum desiccator to remove any further bubbles formed during the pouring process. The PDMS was cured in an oven in ambient air at a temperature of 25 °C for 72 h. Once fully cured, the PDMS negative mold replica was cut using a box cutter and peeled from the template.

A.3 Sensor Assembly

To imprint the PCB sensor with the leaf pattern, the final step requires pressing the negative leaf replica mold into the PCB sensor. A second layer of PDMS was spun at 250 rpm for 60 s to yield a 200 µm layer on the PCB sensor. Next, the negative mold leaf replica was treated with trichloro(1H,1H,2H,2H-perfluorooctyl)silane (PFOCTS) (97% Sigma Aldrich, USA) to act as a non-stick agent. Deposition of PFCOCTS was performed via gas-phase evaporation in a desiccator for 2 h. The treated negative mold leaf replica was then firmly pressed face-down into the coated PCB sensor and was cured in an oven at a temperature of 60°C for 48 h. Once fully cured, the negative leaf replica mold was peeled from the PCB sensor.

A.4 Plasma Treatment

Replica PDMS leaf surfaces required further treatment following sensor assembly. After coating, replica LWS were exposed to oxygen plasma treatment at a base pressure of 40 mTorr, oxygen flow rate of 17.6 sccm, and RF plasma power of 45 W for exposure times varying between 10 - 60 seconds.

A.5 SEM Imaging

All SEM images were taken using a FEI Quanta™ 3D field emission microscope (FEI, USA). Surfaces were observed at a power of 10 kV and spot size of 3.5 nm.

A.6 Contact Angle Measurements

Contact angle measurements were obtained using a VHX-5000 Digital Microscope (Keyence, USA) and analyzed using Image J. Deionized water was used to determine the surface energy of leaves and PDMS leaf replicas. Contact angle of water droplets with a volume of 5µL were recorded.

A.7 Experimental Leaf Wetting Setup

In a natural environment, leaf surfaces are frequently wetted due to dew formation. To achieve the best conditions for dew formation, we created a controlled dew chamber environment where we can regulate meteorological factors including am-

bient temperature and humidity. Furthermore, a Peltier device mounted underneath to control the temperature inducing water droplet condensation. Capacitance measurements were taken using the PCAP02 Capacitance-to-Digital Converter (ScioSense, The Netherlands).